Coexistence of ferroelectric triclinic phases in highly strained $BiFeO_3$ films

Zuhuang Chen,[1] S. Prosandeev,[2] Z. L. Luo,[3] Wei Ren,[2] Yajun Qi,[1] C. W. Huang,[1] Lu You,[1] C. Gao,[3] I. A. Kornev,[5] Tom Wu,[6] Junling Wang,[1] P. Yang,[4] T. Sritharan,[1] L. Bellaiche,[2] and Lang Chen[1,*]

[1]*School of Materials Science and Engineering, Nanyang Technological University, Singapore 639798, Singapore*

[2]*Institute for Nanoscience and Engineering and Physics Department, University of Arkansas, Fayetteville, Arkansas 72701, USA*

[3]*National Synchrotron Radiation Laboratory, University of Science and Technology of China, Hefei, Anhui 230029, People's Republic of China*

[4]*Singapore Synchrotron Light Source (SSLS), National University of Singapore, 5 Research Link, Singapore 117603, Singapore*

[5]*Laboratoire Structures, Proprietes et Modelisation des Solides, Ecole Centrale Paris, CNRS-UMR8580, Grande Voie des Vignes, 92295 Chatenay-Malabry Cedex, France*

[6]*Division of Physics and Applied Physics, School of Physical and Mathematical Sciences Nanyang Technological University, Singapore, 637371, Singapore*

(Received 18 August 2011; published 23 September 2011)

Two tilted *triclinic* phases were found via synchrotron x-ray diffractions in the mixed-phase regions of highly strained $BiFeO_3$ films. First-principles calculations suggest that these two triclinic phases originate from a phase separation of a single monoclinic state accompanied by elastic matching between the two phase-separated states and further suggest that the ease of phase transition between these two energetically close phases is responsible for the large piezoelectric responses observed in Zhang *et al.*, Nat. Nano. **6**, 98 (2011).

DOI: 10.1103/PhysRevB.84.094116 PACS number(s): 77.80.bn, 68.55.aj, 77.55.Nv, 77.80.Jk

I. INTRODUCTION

Ferroelectrics with morphotropic phase boundaries (MPBs) are widely used in actuators and sensors, owing to their excellent piezoelectric properties.[1] Among various ferro/piezoelectrics, $BiFeO_3$ (BFO) is of particular interest due to its lead-free nature, room-temperature multiferroicity, and robust piezoelectricity.[2] Experiments demonstrated that epitaxial strain[3,4] can be used as an alternative to chemical substitution[5] to drive a MPB-like behavior with large piezoresponses in epitaxial BFO films. Two monoclinic ferroelectric phases, tetragonal-like (T-like) M_C and rhombohedral-like (R-like) M_A, have been revealed in the BFO films under large compressive strain.[6,7] A triclinic ferroelectric phase with a large c/a ratio has recently been predicted as a low-energy metastable phase by first principles.[7] This phase with lowest symmetry, if it exists, is particularly interesting as the polarization vector is not constrained by symmetry and is thus free to rotate.[8] In addition the detailed evolution of phase structure with film thickness, the strain-relaxation mechanism, and the origin of enhanced piezoelectric properties in this strain-induced MPB system are not yet fully understood. Furthermore it is known that the structure plays a crucial role on the physical properties of multiferroics due to the spin-charge-lattice coupling.[2,9] It is thus essential to study the structure of highly strained BFO films in details.

To gain insight into the nature of strain-induced phase transitions, we have undertaken synchrotron x-ray diffraction (XRD) experiments, piezoelectric force microscopy (PFM) studies, and first-principles calculations to investigate the structure of BFO films grown on $LaAlO_3$ (LAO) substrates. The complimentary experimental results show that increasing film thickness leads to a phase transformation from a pure T-like phase to a mixture of T-like monoclinic M_C, R-like monoclinic M_A, and two triclinic phases. First-principles calculations suggest an interesting scenario (involving phase separation from a single monoclinic state and elastic matching) for explaining the simultaneous observation of the two triclinic phases, as well as the observed enhancement of piezoelectricity.[3,4]

II. EXPERIMENTAL AND COMPUTATIONAL METHODS

Epitaxial BFO thin films with various thickness were grown on (001) LAO single crystal substrates (CrysTech GmbH) by pulsed-laser deposition with a KrF excimer laser (λ = 248 nm).[10] During growth the substrate temperature was held at 700 °C in oxygen ambient of 100 mTorr. After deposition the samples were slowly cooled to room temperature at a rate of 5 °C/min in 1 atm of oxygen. The thicknesses of films were determined by analysis of synchrotron x-ray reflectivity data and transmission electron microscopy. Conventional $\theta - 2\theta$ XRD investigations were initially done in a four-circle x-ray diffractometer (Panalytical X-pert Pro). Subsequently, high-resolution XRD data were collected at Singapore Synchrotron Light Source (λ = 1.5405 Å) and beam line BL14B1 of the Shanghai Synchrotron Radiation Facility (SSRF) (λ = 1.2398 Å). BL14B1 is a beam line based on a bending magnet, and a Si (111) double-crystal monochromator was employed to monochromatize the beam. The size of the focus spot is about 0.5 mm, and the end station is equipped with a Huber 5021 diffractometer, which is equipped with encoders for its basic four circles (2θ, ω, χ, and ϕ). NaI scintillation detector was used for data collection. The reciprocal space maps (RSMs) were plotted in reciprocal lattice units (r.l.u.) of the LAO substrate (1 r.l.u. = $2\pi/3.789$ Å^{-1}). PFM investigations were carried out on an Asylum Research MFP-3D atomic force microscope (AFM) using TiPt-coated Si tips (DPE18, MikroMasch). The PFM images have been recorded with the tip cantilever pointing along ⟨100⟩ direction.

We performed density-functional calculations (DFT)[11] using the Vienna *ab-initio* simulation package (VASP)[12] within the local spin density approximation plus the Hubbard parameter U (LSDA+U) with U = 3.87 eV.[13,14] We used the projected

augmented wave (PAW) method and a $2 \times 2 \times 2$ k-point mesh and an energy cutoff of 500 eV. We employed a 40-atom cell, in which either a G-type or C-type antiferromagnetic order is assumed. In order to mimic (001) epitaxial BFO films we adopted the following lattice vectors for this 40-atom unit cell, as given in the Cartesian (x, y, z) setting for which the x, y, and z-axes are along the pseudocubic [100], [010], and [001] directions, respectively, by $\vec{a_1} = 2a(1,0,0)$, $\vec{a_2} = 2a'(0,1,0)$, $\vec{a_3} = 2a(\Delta_1, \Delta_2, 1 + \Delta_3)$, where a and a' are both in-plane lattice parameters. For each considered value of these in-plane lattice constants, the Δ_1, Δ_2, Δ_3 variables and internal atomic coordinates are relaxed to minimize the total energy, the Hellman-Feynman forces and some components of the stress tensor. Note that, in the following, we rescaled our lattice parameters by a ratio of 1.0154 in order to account for the underestimation of the LSDA+U method.

III. RESULTS AND DISCUSSION

Figure 1(a) shows a representative AFM topography of a 10-nm-thick BFO film. Atomically flat terraces with single-unit-cell-high steps are observed, indicating the layer-by-layer growth. As shown in Fig. 1(b), only 00l diffraction peaks of the film and substrate were observed in the θ–2θ XRD pattern, indicating epitaxial growth. The out-of-plane lattice parameter of BFO is calculated to be $c \sim 4.64$ Å, which demonstrates the stabilization of T-like phase.[15] The presence of thickness fringes [Fig. 1(b)] indicates a high crystalline quality and smooth surface. It is known that the flat area in AFM topography correspond to the pure T-like phase and the stripe-like area correspond to the mixed phase.[3] The absence of stripe-like contrast in Fig. 1(a) further suggests that the ultra-thin film consists of the T-like phase only. With increasing film thickness the stripe-like area of the mixed phase emerges to relieve strain.[3,10] The striped features are clearly observed in the topographic image of a ~80-nm-thick film in Fig. 1(c). The phase coexistence can also be identified through $\theta - 2\theta$ diffractogram, as shown in Fig. 1(d). The out-of-plane c-lattice parameters calculated from the position of the 00l peaks are ~3.97 Å and ~4.67 Å for the R-like and T-like phases, respectively, which are in agreement with earlier studies.[6,10] Another phase (labeled as Tri-1) with a c parameter of ~4.18 Å was detected as well [Fig. 1(d)].

To clarify the structure of the film, high-resolution synchrotron XRD was employed. Figure 2(a) shows a HL-plane mapping near the 002 diffraction for the 80-nm-thick film (H, K, and L are reciprocal space coordinates). Diffraction peaks from the T-like ($L \sim 1.624$) and R-like phases ($L \sim 1.907$) were found to have the same H value as that of the substrate, indicating that there is no tilt between the (001) plane of these two phases and the substrate. Besides the peaks of the R-like and T-like phases, two additional sets of peaks were observed, which included two sets of peak pairs with same L value but opposite H values. The first set with $L \sim 1.812$ corresponds to the Tri-1 phase, which has a c-lattice parameter of 4.178(1) Å, and it is tilted by an angle of $\pm 2.7^\circ$ ($H \sim \pm 0.087$) into the [100] direction with respect to the substrate surface normal. The second set of two peaks with $L \sim 1.619$ corresponds to another phase (labeled as Tri-2), which has a c-lattice parameter of 4.682(2) Å and a tilt angle of $\pm 1.5^\circ$ ($H \sim \pm 0.042$) along

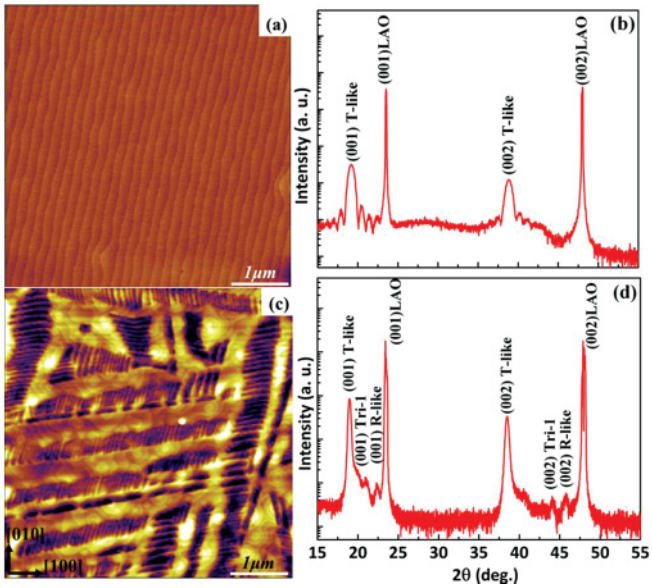

FIG. 1. (Color online) (a) AFM topography and (b) XRD $\theta - 2\theta$ scan of a 10-nm-thick BFO film on LAO substrate. (c) AFM topography and (d) XRD $\theta - 2\theta$ scan of an 80-nm-thick BFO film on LAO.

the [100] direction. These two sets of diffraction peaks have also been observed in a very recent paper.[16] As shown in Fig. 2(b), the $\bar{1}03$ diffraction peak of the T-like phase splits into three adjacent peaks, indicating that the T-like phase is monoclinic M_C.[6,7,17] This is further confirmed by in-plane domain image as presented in Fig. 2(c). A stripe-like domain structure aligned along the ⟨110⟩ direction is clear in the flat T-like area, indicating that the polarization vector of the T-like phase lies within the (010) plane.[6,17] The lattice parameters of the T-like phase extracted from the ($\bar{1}03$) RSM are $a_m = 3.811(1)$ Å, $b_m = 3.734(2)$ Å, $c_m = 4.670(2)$ Å, and $\beta = 88.23(2)^\circ$. Strikingly, the intensity of diffraction of the R-like phase is very weak compared with the other three phases (Tri-1, Tri-2, and T-like) and were even not detected in other studies,[9] suggesting that the fraction of the R-like phase must be very small.

To get more detailed information on spatial arrangements of the two tilted phases, plan-view HK mappings were obtained around (002) peak with L values at the peaks of the tilted phases, shown in Figs. 2(d) and 2(e). Interestingly, the RSMs clearly exhibit eight peaks with tilt angles along both the H and K directions in both figures. Note that the central strong peak in Fig. 2(e) is from the T-like phase due to the close c parameters of the T-like and Tri-2 phases. The tilt angles are determined to be $\pm 2.7^\circ$ along [100] (or [010]) direction and $\pm 0.5^\circ$ along [010] (or [100]) direction for the Tri-1 phase, and $\pm 1.5^\circ$ along [100] (or [010]) direction and $\pm 0.4^\circ$ along [010] (or [100]) direction for the Tri-2 phase. The eight diffraction spots in the plan-view mappings are consistent with the observation of eight orientations of stripe-like features on the film surface.[18] The schematic domain arrangement of the tilted phases is shown in Fig. 2(f). The presence of eight spots simultaneously in both Tri-1 and Tri-2 phases demonstrates the affinity between the two phases. Further taking into account a small fraction of the R-like phase, we suggest that the

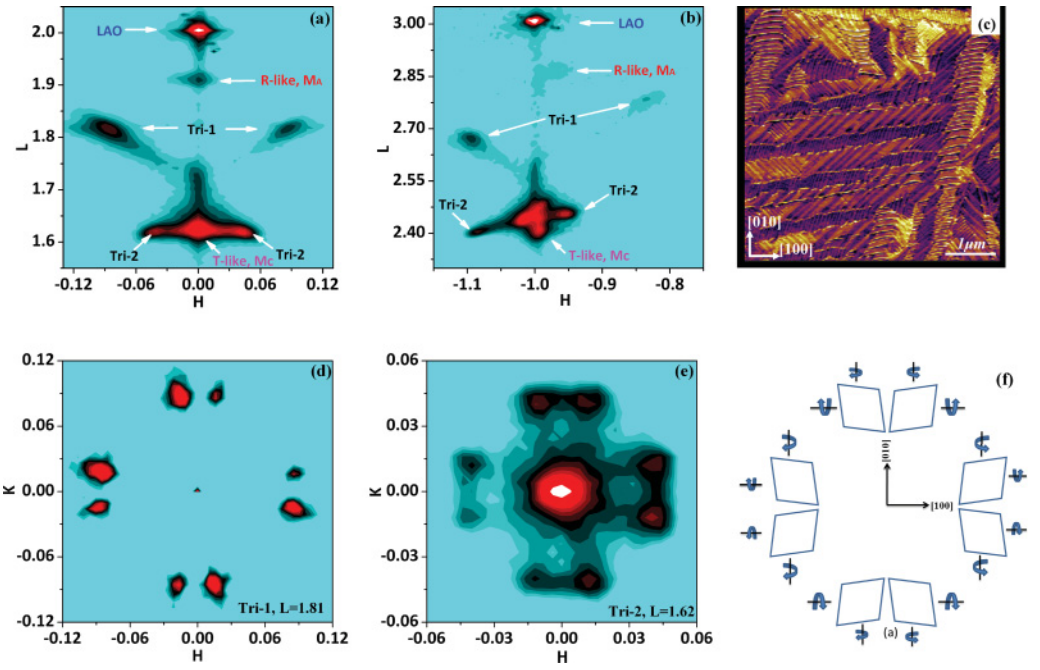

FIG. 2. (Color online) (a) (002) and (b) ($\bar{1}03$) *HL*-plane RSM of the 80-nm-thick BFO film on LAO. (c) In-plane PFM image of the 80-nm-thick BFO film. (002) *HK*-plane RSM at (d) $L = 1.81$ (Tri-1 phase) and (e) $L = 1.62$ (Tri-2 phase) of the film. (f) Schematic of real-space domain pattern of the tilted triclinic phases.

mixed-phases regions are made up not of the R- and T-like phases, as reported previously,[3,10] but of an intimate mixture of the two triclinic tilted phases. A similar conclusion has also been made in a very recent study by using high resolution AFM.[16] Due to low resolution along *K* direction, four peaks of the Tri-1 phase are observed instead of two in the (002) *HL* mapping by conventional XRD.[9,16] In addition the reason why previous studies[3,10] using $\theta - 2\theta$ scan did not detect the Tri-1 phase is probably attributable to the large tilt angle.

The determination on lattice parameters and crystal system of the two-tilted Tri-1 and Tri-2 phases is using simplified 3-dimensional (3D) reciprocal space mapping at synchrotron radiation sources. The so-called simplified 3D reciprocal space mapping is used to precisely measure the coordinates for several reciprocal space vectors (RSVs) [(002), ($\bar{1}03$), and (013)] only instead of doing whole 3D mappings in order to save time. Mathematical operation of these RSVs will lead to reduction of three basis vectors, $\boldsymbol{a}^*$, $\boldsymbol{b}^*$, and $\boldsymbol{c}^*$ in the reciprocal space. The lengths and angles of $\boldsymbol{a}$, $\boldsymbol{b}$, and $\boldsymbol{c}$ can subsequently be obtained in the real space, and hence the crystal system is determined (diffraction-intensity symmetrical study is necessary). Such measurement on RSVs can firmly deduce the angles with higher precisions between the basis axes, whereas bigger errors might be introduced, for example, using *d*-value method, or it is taken as 90° for granted in some 2D-mapping cases. We set a Cartesian coordinate system first in crystal reciprocal space using a reciprocal lattice unit (1 r.l.u. $= 2\pi/3.789$ Å^{-1}). Such a system can be set using the SPEC control software. The corresponding lattice parameter is close to those of LAO substrate, that is $a = 3.790$ Å and $\alpha = 90.09°$. Note that the use of orthogonal coordinate system is convenient to do calculation and relieves some troubles from twinning in a reference such as the substrate. Similiar procedure was applied to lattice-parameter determination for the two-tilted phases of BFO films. The key point is to obtain the angle γ between $\boldsymbol{a}$ and $\boldsymbol{b}$ if $\boldsymbol{c}$ is assigned along the normal of the film. Careful measurements proved that $\boldsymbol{a}$ or $\boldsymbol{b}$ of the two tilted phases of BFO was not located or parallel to any coordinate plane (*xz*, *yz*, or *xy* plane). The coordinate data of the LAO substrate and two tilted phases are listed in Table I.

Combining all diffraction data, we can unambiguously determine the lattice parameters and crystal symmetries of the two tilted phases. Both phases can be concluded as belonging to the triclinic system, rather than monoclinic system as claimed in a recent study,[16] from the calculations of the lengths and angles between the crystal axes. The typical lattice parameters of the tilted phase are: $a_{\mathrm{Tri-1}} = 3.911(2)$ Å,

TABLE I. Coordinate data in reciprocal space of the LAO substrate, Tri-1 and Tri-2 phases.

	LAO	Tri-1	Tri-2
(002)	(0.0000, 0.0000, 2.0000)	(−0.08756, −0.01396, 1.8117)	(−0.0415, −0.0103, 1.6194)
($\bar{1}03$)	(−1.0010, 0.0004, 2.9999)	(−1.0986, −0.01175, 2.6707)	(−1.0811, −0.0148, 2.4065)
(013)	(0.0006, 1.0004, 3.0025)	(−0.1323, 0.9708, 2.7345)	(−0.0638, 0.9777, 2.4081)

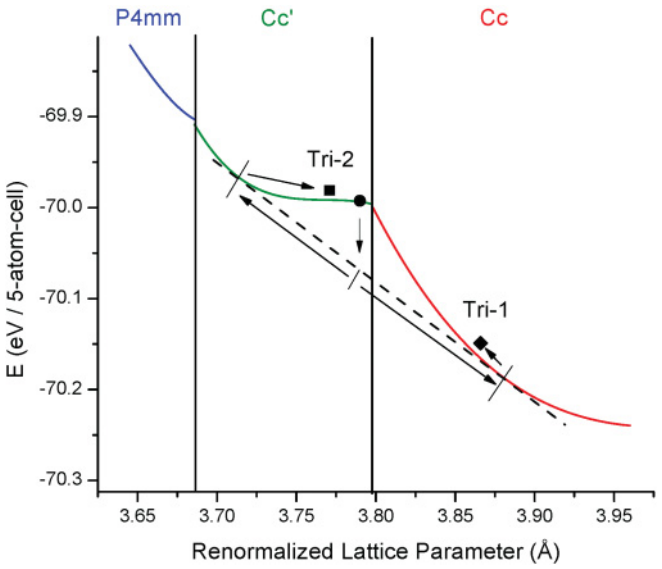

FIG. 3. (Color online) Total energy versus the in-plane lattice parameter of the equilibrium phases in an epitaxial (001) BFO film. The red, green, and blue curves represent the Cc, Cc', and $P4mm$ phases, respectively. The filled black symbols show the energies of the Tri-1 and Tri-2 phases at their average $(a + a')/2$ in-plane lattice parameter. The dashed line is tangent to the Cc and Cc' energy curves. The arrows schematized the proposed phase-separated mechanism to explain the existence of the Tri-1 and Tri-2 phases.

$b_{\mathrm{Tri}-1} = 3.822(1)$ Å, $c_{\mathrm{Tri}-1} = 4.178(1)$ Å, $\alpha_{\mathrm{Tri}-1} = 89.47(4)^\circ$, $\beta_{\mathrm{Tri}-1} = 89.91(7)^\circ$, and $\gamma_{\mathrm{Tri}-1} = 89.45(2)^\circ$ for Tri-1; and $a_{\mathrm{Tri}-2} = 3.816(2)$ Å, $b_{\mathrm{Tri}-2} = 3.720(1)$ Å, $c_{\mathrm{Tri}-2} = 4.682(2)$ Å, $\alpha_{\mathrm{Tri}-2} = 88.49(6)^\circ$, $\beta_{\mathrm{Tri}-2} = 89.78(4)^\circ$, and $\gamma_{\mathrm{Tri}-2} = 89.84(2)^\circ$ for Tri-2. It is found that the unit-cell volume of the Tri-1 phase is near that of the R-like (∼62.3 Å^3),[6] and Tri-2 is near that of T-like (∼66.4 Å^3). Therefore, we deduce that the Tri-1 phase should evolve from the R-like M_A phase and is highly distorted and tilted, while Tri-2 phase should originate from the T-like M_C phase.

Recent theoretical studies have shown that several phases are potentially stable in BFO films.[7,19] In order to theoretically support the existence and coexistence of the two triclinic phases, we performed DFT calculations. We first concentrate on *perfect* epitaxial conditions, that is $a = a'$. Figure 3 shows the energy versus the in-plane lattice constant a for the equilibrium phases only for the compressive strain. In agreement with previous works[20,21] three ground-state phases are predicted to occur for these ideal epitaxial conditions: (1) a monoclinic Cc state with a G-type antiferromagnetic ordering for a ranging between 3.96 Å and 3.80 Å. This Cc state has both a polarization and axis about which the oxygen octahedral tilt in antiphase lying along [uuv] directions. (2) Another monoclinic state that also has a Cc space group but that will be denoted as Cc' in the following to differentiate it from the first Cc phase for a ranging between 3.80 Å and 3.68 Å. This Cc' state exhibits a large axial ratio and a large out-of-plane component polarization in addition to small in-plane components of the polarization and small oxygen octahedral tilting. It also possesses a C-type antiferromagnetic ordering, rather than a G-type as in Cc. (3) A tetragonal $P4mm$ phase (with also a C-type antiferromagnetic ordering), which possesses a large axial ratio and a large polarization fully lying along the [001] pseudocubic direction, for smaller in-plane lattice constants. As one can see from Fig. 3, no triclinic ground-state is found from these simulations.

However, if we allow the two in-plane lattice constants a and a' to be of different magnitude and equal to those experimentally seen, two triclinic phases indeed emerge as ground states from these new epitaxial conditions after relaxation of the atoms and cell variables. The energy of these two triclinic states is indicated in Fig. 3 for their $(a + a')/2$ average lattice constant. Table II shows the lattice vectors of these two triclinic phases, which demonstrates that they are indeed the Tri-1 and Tri-2 state experimentally observed since one triclinic state has a c parameter around 4.1 Å (close to that of the corresponding parameter in the experimental Tri-1 phase), while the other triclinic phase has a predicted large c parameter equal to 4.68 Å (exactly as in the observed Tri-2 phase). Table II also provides the Cartesian components of the polarization and of the antiferrodistortive vector whose direction represents the axis about which the oxygen octahedral tilt in antiphase fashion and whose magnitude provides the angle of such tilting.[14] Note that the antiferromagnetic ordering of the Tri-1 phase is found to be of G-type (like the Cc states), while it is of C-type for the Tri-2 state (like the Cc' phases).

Why are these triclinic states, rather than the Cc and Cc' phases, experimentally observed when growing relatively thick BFO film on LAO? It is important to realize that the lattice constant of LAO is 3.79 Å, as shown in Fig. 3, and yields a Cc' ground state. Interestingly, for this lattice constant, the energy of this particular Cc' phase is higher than the energy associated with the dashed line that is tangent to the energy-versus-lattice constant curves of the Cc and Cc' phases (this tangent line

TABLE II. Physical properties of the Tri-1 and Tri-2 phases. For comparison these properties are also given in a Cc phase for which the in-plane lattice constant is the average of the in-plane lattice parameters of the Tri-1 and Tri-2 phases. The polarization is estimated from the relaxed atomic displacements and calculated Born effective charges.

Physical properties	Tri-1	Tri-2	Cc
40-atom cell lattice vectors divided by 2 (Å)	(3.911, 0.000, 0.000)	(3.721, 0.000, 0.000)	(3.818. 0.000. 0.000)
	(0.000, 3.821, 0.000)	(0.000, 3.821, 0.000)	(0.000, 3.818, 0.000)
	(−0.014, −0.006, 4.072)	(0.107, 0.139, 4.680)	(−0.014, −0.014, 4.173)
Polarization, C/m^2	(0.471, 0.399, 0.661)	(0.236, 0.293, 1.585)	(0.391, 0.391, 0.817)
Antiferrodistortive vector, Radian	(0.139, 0.125, 0.167)	(0.043, 0.046, 0.004)	(0.120, 0.120, 0.177)
Piezoelectric coefficient e_{33} (C/m^2)	3.6	1.9	4.9

intercepts these curves at around 3.72 Å and 3.88 Å). Because relatively thick BFO films can relax with respect to perfect epitaxial conditions, it is thus energetically more favorable for (001) BFO films grown on LAO to phase separate into a Cc state with an in-plane lattice constant $a = 3.88$ Å and a Cc' state having $a = 3.72$ Å.[22] However, these two phase-separated Cc and Cc' states have to elastically match each other since they have to coexist in the same sample (as neighboring domains). This elastic matching forces each of these states to exhibit two different in-plane parameters, a and a', rather than a single one. As a result, this Cc state with $a = 3.88$ Å becomes the Tri-1 state shown in Table II while the Cc' state with $a = 3.72$ Å transforms into Tri-2 (note that this elastic matching is further suggested by realizing that the Tri-1 and Tri-2 phases have the same a' in-plane parameter while their average a parameter is also equal to this a' value). This explains why coexisting domains made of Tri-1 and Tri-2 phases are observed in thick-enough BFO films grown on LAO.

Let us now concentrate on the piezoelectric responses of the Tri-1 and Tri-2 phases. Table II reveals that, according to first-principles calculations, the two triclinic phases have e_{33} piezoelectric coefficients that are significant but not that huge, despite the fact that their polarizations do not lie along a high-symmetry direction and is therefore free to move/rotate along any direction. The $T = 0$ K magnitude of these e_{33} coefficients are about 2–4 C/m^2, which is of the same order than that in typical ferroelectrics such as $PbTiO_3$.[23] In fact Table II further shows that the e_{33} coefficients of Tri-1 and Tri-2 are smaller than the corresponding coefficient of the Cc phase that has an in-plane lattice constant that is the average between the a and a' lattice constants of Tri-1 and Tri-2. It is likely that applying an electric field in a film in which the Tri-1 and Tri-2 phases coexist as alternating domains will move the phase boundary between these two phases and thus result in giant piezoelectric responses (since Tri-1 and Tri-2 have c lattice parameters that differ by nearly 10%). Such a prediction is in line with the fact that the pure T-like and R-like phases of BFO have been found to have much smaller piezoelectricity with respect to mixed-phase samples made of alternating so-called T/R domains.[4]

The ease of phase transition between two triclinic phases can also be derived through the presence of diffuse scattering peaks connecting the diffraction peaks of these two phases, as shown in Figs. 2(a) and 2(b). This spread of peaks can be attributed to a transition region with lattice parameter gradient between the two tilted phases in which the polarization can rotate from the Tri-1 phase to Tri-2 phase, as shown in Fig. 4, which might effectively relieve epitaxial strain during phase transition. Therefore, it is not always necessary to involve dislocations to relieve misfit strain, as shown that within ten unit cells, a defect-free phase boundary has been observed with continuously changing c parameters in a TEM picture.[3]

Generally speaking, it is usually difficult to clarify the mechanism of enhanced piezoelectricity near MPB, mainly due to the complex chemistry, ambiguity of structure, and disorder nature in lead oxide-based solid solutions.[24] The lattice parameters of these solid solutions are metrically close to cubic, which lead to subtle differences among the crystal symmetries of possible phases.[25] For instance, the phase

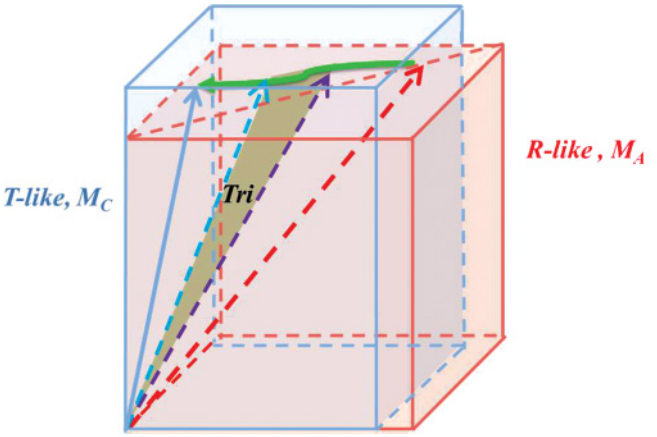

FIG. 4. (Color online) Schematic of polarization rotation path between T-like M_C (blue) and R-like M_A (red) phases. The grey shaded region is the phase boundary between the two tilted triclinic phases.

diagram of prototypical PZT solid solution, especially near MPB, is still controversial, and a lot of different models are proposed to explain the mechanism of enhanced piezoelectric response near MPB.[26] There are some discussions over whether the presence of monoclinic structure or nanodomains is a necessary or sufficient condition for large piezoelectric response. Herein, we suggest that the strained BFO films provide an alternative perspective to verify the role of nanodomains and low-symmetry phases on the enhanced piezoelectric response. Despite the presence of nanodomains and its monoclinic nature,[6] pure T- or R-like phase BFO films exhibit much smaller piezoelectric properties than mixed-phase ones.[4] Therefore, our works suggest that the sole presence of monoclinic phase or nanodomains may not be sufficient to provide large piezoelectric response. The large piezoelectric response shall be related to free-energy instability and to the ease of polarization rotation or phase transition under external stimuli.[27] The coexisting phase-separated triclinic phases in the highly-strained BFO films are able to bridge the T-like M_C and R-like M_A phases and thus facilitate the field-induced phase transition, as shown in Fig. 4, thus resulting in large piezoelectric response observed in the Refs. 3 and 4. Similar polarization rotation path (M_A-Tri-M_C) has also been reported in the PZT solid solution under electric field.[28]

IV. CONCLUSION

In summary we provide direct evidences for the existence of two different triclinic phases in highly strained multiferroic $BiFeO_3$ films through careful structural studies and detailed first-principles calculations. Our results suggest that the stripe-like mixed-phases regions are mainly made up of two highly tilted triclinic phases that originate from (1) a phase separation from a single monoclinic state and (2) elastic matching. We propose that a large piezoelectric response should arise from the ease of field-induced phase transition between these two energetically close phases. These findings enrich the knowledge of the lattice and domain structure in epitaxial BFO

films, and also shed some light on mechanisms for enhanced electromechanical coupling near MPB.

ACKNOWLEDGMENTS

L.C. acknowledges the support from AcRF RG 21/07, ARC 16/08, MINDEF-NTU-JPP 10/12 and NRF CREATE HUJ-BGU-NTU. L.B. mostly acknowledges ONR Grants N00014-11-1-0384 and N00014-08-1-0915 for financial support. NSF grant DMR-0701558 and DMR-0080054 (C-SPIN), and the Department of Energy, Office of Basic Energy Sciences, under contract ER-46612, are also acknowledged for discussions with scientists sponsored by these grants. Some computations were also made possible thanks to the MRI grant 0959124 from NSF, N00014-07-1-0825 (DURIP) from ONR and a Challenge grant from HPCMO of the US Department of Defense. P.Y. would like to thank the support from SSLS via NUS Core Support C-380-003-003-001. The authors thank Eddie Chu and J. Íñiguez for useful discussions and beamline BL14B1 (SSRF) for providing the beam time under Project No. j10sr0092.

*Corresponding author: langchen@ntu.edu.sg

[1] K. Uchino, *Ferroelectric Devices* (Dekker, New York, 2000).
[2] G. Catalan and J. F. Scott, Adv. Mater. **21**, 2463 (2009).
[3] R. J. Zeches, M. D. Rossell, J. X. Zhang, A. J. Hatt, Q. He, C.-H. Yang, A. Kumar, C. H. Wang, A. Melville, C. Adamo, G. Sheng, Y.-H. Chu, J. F. Ihlefeld, R. Erni, C. Ederer, V. Gopalan, L. Q. Chen, D. G. Schlom, N. A. Spaldin, L.W. Martin, and R. Ramesh, Science **326**, 977 (2009).
[4] J. X. Zhang, B. Xiang, Q. He, J. Seidel, R. J. Zeches, P. Yu, S. Y. Yang, C. H. Wang, Y. H. Chu, L. W. Martin, A. M. Minor, and R. Ramesh, Nat. Nano. **6**, 98 (2011).
[5] S. Fujino, M. Murakami, V. Anbusathaiah, S. H. Lim, V. Nagarajan, C. J. Fennie, M. Wuttig, L. Salamanca-Riba, and I. Takeuchi, Appl. Phys. Lett. **92**, 3 (2008).
[6] Z. H. Chen, Z. L. Luo, C. W. Huang, Y. J. Qi, P. Yang, L. You, C. H. Hu, T. Wu, J. L. Wang, C. Gao, T. Sritharan, and L. Chen, Adv. Funct. Mater. **21**, 133 (2011).
[7] H. M. Christen, J. H. Nam, H. S. Kim, A. J. Hatt, and N. A. Spaldin, Phys. Rev. B **83**, 144107 (2011).
[8] D. Vanderbilt and M. H. Cohen, Phys. Rev. B **63**, 094108 (2001).
[9] Q. He, Y. H. Chu, J. T. Heron, S. Y. Yang, W. I. Liang, C. Y. Kuo, H. J. Lin, P. Yu, C. W. Liang, R. J. Zeches, W. C. Kuo, J. Y. Juang, C. T. Chen, E. Arenholz, A. Scholl, and R. Ramesh, Nat. Commun. **2**, 225 (2011).
[10] Z. H. Chen, L. You, C. W. Huang, Y. J. Qi, J. L. Wang, T. Sritharan, and L. Chen, Appl. Phys. Lett. **96**, 252903 (2010).
[11] W. Kohn and L. J. Sham, Phys. Rev. A **140**, 1133 (1965).
[12] G. Kresse and J. Furthmüller, Phys. Rev. B **54**, 11169 (1996).
[13] V. Anisimov, F. Aryasetiawan, and A. Lichtenstein, J. Phys. Condens. Matter **9**, 767 (1997).
[14] I. A. Kornev, S. Lisenkov, R. Haumont, B. Dkhil, and L. Bellaiche, Phys. Rev. Lett. **99**, 227602 (2007).
[15] H. Bea, B. Dupe, S. Fusil, R. Mattana, E. Jacquet, B. Warot-Fonrose, F. Wilhelm, A. Rogalev, S. Petit, V. Cros, A. Anane, F. Petroff, K. Bouzehouane, G. Geneste, B. Dkhil, S. Lisenkov, I. Ponomareva, L. Bellaiche, M. Bibes, and A. Barthelemy, Phys. Rev. Lett. **102**, 217603 (2009).
[16] A. R. Damodaran, C.-W. Liang, Q. He, C.-Y. Peng, L. Chang, Y.-H. Chu, and L. W. Martin, Adv. Mater. **23**, 3170 (2011).
[17] Z. H. Chen, Z. L. Luo, Y. J. Qi, P. Yang, S. X. Wu, C. W. Huang, T. Wu, J. L. Wang, C. Gao, T. Sritharan, and L. Chen, Appl. Phys. Lett. **97**, 242903 (2010).
[18] H. Y. Kuo, Y. C. Shu, H. Z. Chen, C. J. Hsueh, C. H. Wang, and Y. H. Chu, Appl. Phys. Lett. **97**, 242906 (2010).
[19] O. Diéguez, O. E. González-Vázquez, J. C. Wojdeł, and J. Íñiguez, Phys. Rev. B **83**, 094105 (2011).
[20] A. J. Hatt, N. A. Spaldin, and C. Ederer, Phys. Rev. B **81**, 054109 (2010).
[21] J. C. Wojdeł and J. Íñiguez, Phys. Rev. Lett. **105**, 037208 (2010).
[22] A. L. Roytburd and J. Ouyang, Fundamental *Physics of Ferroelectrics and Related Materials 2011*, National Institute of Standards and Technology, Gaithersburg, MD, Jan 30–Feb. 2, 2011.
[23] L. Bellaiche and D. Vanderbilt, Phys. Rev. Lett. **83**, 1347 (1999).
[24] M. Ahart, M. Somayazulu, R. E. Cohen, P. Ganesh, P. Dera, H.-K. Mao, R. J. Hemley, Y. Ren, P. Liermann, and Z. G. Wu, Nature **451**, 545 (2008).
[25] B. Noheda, Curr. Opin. Solid State Mat. Sci. **6**, 27 (2002).
[26] D. Damjanovic, IEEE Trans. Ultrason. Ferroelectr. Freq. Control **56**, 1574 (2009).
[27] D. Damjanovic, Appl. Phys. Lett. **97**, 062906 (2010).
[28] L. Bellaiche, A. Garcia, and D. Vanderbilt, Phys. Rev. B **64**, 060103 (2001).